Reflectometry fluctuation diagnostics at Wendelstein 7-X

T. Windisch[1], T. Estrada[2], M. Hirsch[1], W. Kasparek[3], A. Krämer-Flecken[4], C. Lechte[3], S. Wolf[3], P. Xanthopoulos[1] and T. Klinger[1]

[1] *Max-Planck-Institute for Plasma Physics, Greifswald, Germany*

[2] *Centro de Investigationes, Medioambientales y Technologicas (CIEMAT), Madrid, Spain*

[3] *Inst. für Grenzflächenverfahrenstechnik und Plasmatechnologie, Univ. Stuttgart, Germany*

[4] *Institut für Energie- und Klimaforschung, Forschungszentrum Jülich, Germany*

Wendelstein 7-X, the first superconducting stellarator along the five-fold symmetric HELIAS line, will start operation in fall this year. In its first commissioning operation phase (OP1.1) plasma energy is limited to 2 MJ, which corresponds to a pulse length of 0.4 s at 5 MW ECR-heating. The plasma boundary with open flux surfaces is produced by five graphite inboard limiters in order to protect in-vessel components. In the second operation phase (OP1.2), an inertially cooled island divertor and a water cooled first wall allow 10 s operation at 10 MW heating power. Finally, in OP2, scheduled to start in 2019, 1800s pulses with 10 MW are envisaged using water cooled island divertors.

From the beginning, a set of microwave reflectometry systems dedicated to measure the spatio-temporal evolution of density fluctuations are operated, i.e, a V-band Doppler reflectometer (DR, provided by CIEMAT) and a Ka-band poloidal correlation reflectometer (PCR, provided by FZ Jülich). In the later operation phases, the DR will be extended to the W-band, and a novel steerable Doppler reflectometer (SDR, developed at IVGP Stuttgart) will be installed. The systems are briefly described in the following. All reflectometer systems are designed to measure fluctuations localized around the last closed flux surface (LCFS), where large variations

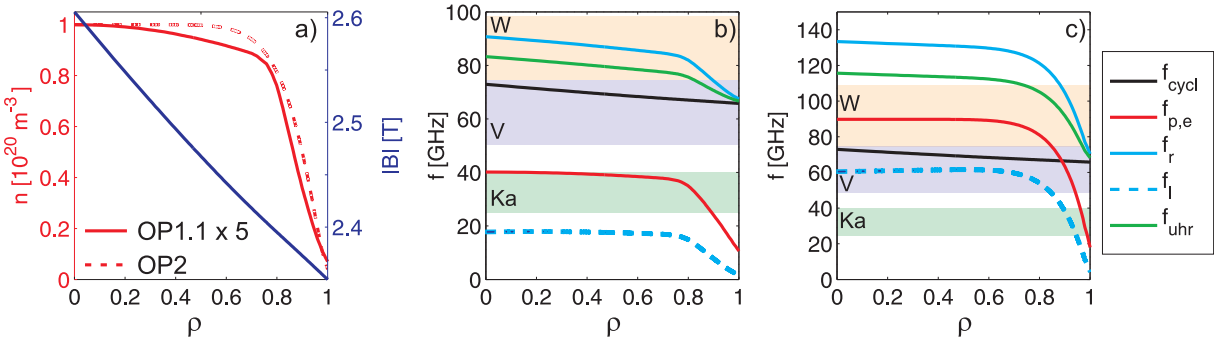

Figure 1: (a) Assumed radial profiles of n and |B| (solid: scenario OP1.1, dashed: scenario OP2), and (b-c) corresponding resonance and cut-off frequencies for sc. OP1.1 and sc. OP2. The used microwave bands are shown as colored boxes.

in the perpendicular $E_r \times B_t$-flow are expected.

Assumed density profiles for two operation scenarios (scenario OP1.1, scenario OP2) are shown in Fig. 1a. In scenario OP2, the expected peak density is approx. five times larger than in scenario OP1.1. The reflectometer systems are located in one of the five highly elongated corners of W7-X, the so-called bean shaped plane ($\phi = 72°$). Typical flux-surfaces and the design beam paths of the DR and PCR are shown in Fig. 2. The design cut-off positions are around the outer midplane. In contrast to a tokamak, the outer midplane is not a bad curvature region for all toroidal locations per se. For the bean shaped and triangular shaped planes of W7-X, the normal magnetic field curvature κ is shown in Fig. 3 along the magnetic field lines crossing the respective planes at poloidal angle $\theta = 0$ (blue line). Also shown are the mode structures associated with ITG fluctuations as obtained from linear GENE simulations with adiabatic electrons (red lines). Around the outer midplane ($\theta = 0$) the poloidal structure of the fluctuations differs significantly. In the case of the bean shaped plane the fluctuations peak at the design cut-off position ($z = 0$). This theoretical prediction could be proven directly utilizing the reflectometry systems.

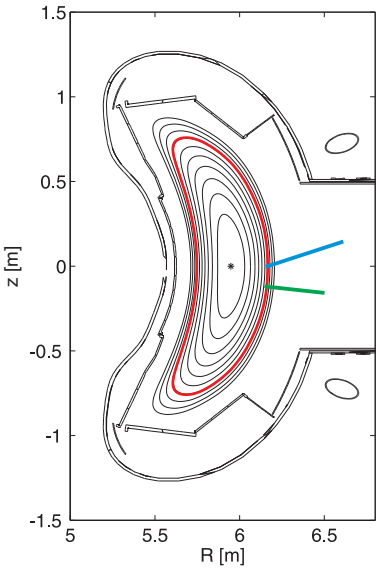

Figure 2: Flux surfaces and DR (blue) and PCR (green) beam paths.

The broadband DR system operates in V- and W-band ($50 - 110\,\mathrm{GHZ}$) using o- or x-mode polarization. The corresponding cut-off positions for OP1.1 and OP2 are shown in Fig. 1b-c. The measurement principle relies on the Bragg backscattering mechanism. Via the Bragg condition $k_\perp = 2k_0 \sin(\theta_{\mathrm{tilt}})$ fluctuations with $k_\perp$ are selected out of the turbulent spectrum at

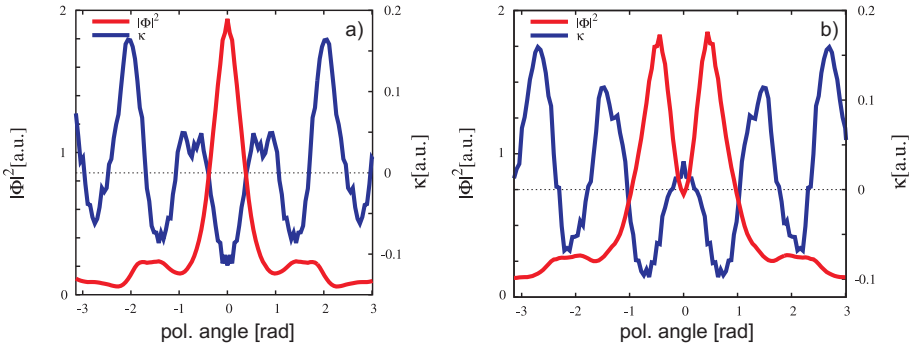

Figure 3: Normal magnetic field curvature κ (blue) and ITG potential fluctuations (red) on a flux surface for the (a) bean and (b) triangular shaped plane as obtained from linear GENE runs (taken from Ref. [1]).

the cutoff-layer. The bistatic system has a fixed incidence angle to the flux surface normal $\theta_{tilt} = \pm 18°$. The design cutoff is located at $\rho = 0.85$, which is 4 cm inside the LCFS. This flux surface is highlighted in Fig. 2 as orange line . The chosen tilt angle is a compromise between path length (beam waist, damping), suppression of the strong $m = 0$ scattering component and desired wavenumber. The chosen angle corresponds for $f = 80$ GHz to $\lambda_\perp = 0.6$ cm. The accessible wavenumber range as computed with TRAVIS [2] is shown in Fig. 4. Since the measured signal is Doppler shifted, it allows to estimate the perpendicular velocity of the fluctuations (provided $k_\parallel \ll k_\perp$). In order to enhance the wavenumber resolution and to ensure a broadband operation of the DR system, special attention has been paid to the Gaussian antenna system, which consists of six mirrors. Details about the optimization strategy can be found in Ref. [3]. The O-mode PCR system consists of five antennae, i.e. one launching and four receiving antennae [4]. With a cut-off density $n_c = 2 \cdot 10^{19}\,\mathrm{m}^{-3}$ it measures in sc. OP2 around the LCFS $\rho = 0.96 - 0.98$. Via correlation techniques the poloidal propagation and correlation lengths and times of the turbulent structures can be analyzed. In addition the occurrence of (quasi-)coherent modes may be measured directly and the pitch angle of the local magnetic field can be estimated.

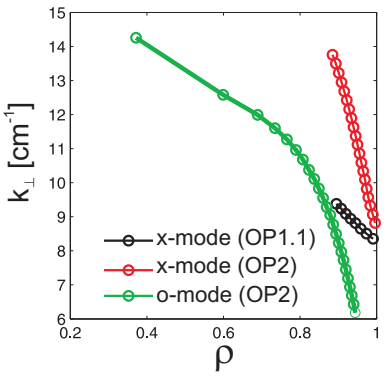

Figure 4: Accessible perpendicular wavenumber of the DR system.

The SDR system allows to change the incidence angle θ_{tilt} and thereby scanning a part of the wavenumber spectra without any movable parts in the vacuum. This is achieved by a phased-array antenna consisting of 32 stacked H-plane sectoral horns [5]. The phased feed array allows to tilt angle between $\pm 20°$ by a small frequency change $\Delta f \approx 700$ MHz at around 15 frequencies in the W-band. The offset tilt angle is chosen to allow a direct comparison with the DR system. The accessible radial and wavenumber range as estimated with TRAVIS is shown in Fig. 5.

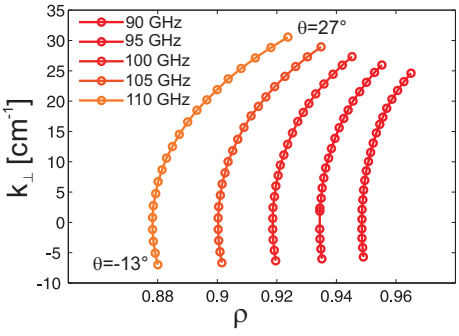

Figure 5: Accessible perpendicular wavenumber of the SDR system.

In general the interpretation of the measurement signals is often quite challenging due to the complex interplay between microwave reflection, scattering (multiple), refraction and mode coupling, especially for larger fluctuation amplitudes. Here, full wave calculations can be used

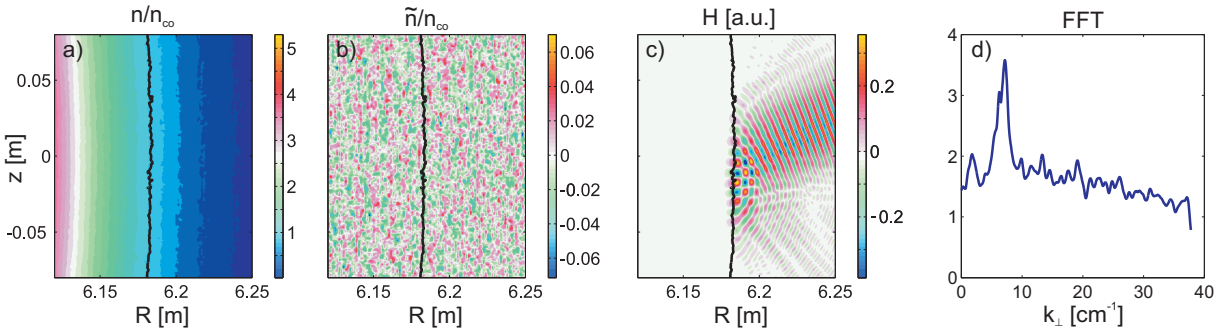

Figure 6: Normalized density (a) and density fluctuations (b) as obtained from GENE simulations, full wave simulation (c), and radially averaged spectra of density fluctuations (d).

to gain a better understanding. For this purpose we use the IPF-FD3D code developed at the University of Stuttgart [6]. The input density fluctuations for the full wave code is taken from flux-surface GENE simulations [7] at $\rho = 0.8$, which then defines the cut-off layer position and microwave frequency, respectively. Note, that in the domain of the flux surface simulations ($x = 264\,\rho_s \sim 25\,\mathrm{cm}$ for $T_e = 254\,\mathrm{eV}$) the radial density and temperature gradients are assumed to be constant. The density and fluctuations in the interesting full wave domain are shown in Fig. 6a,b. Both are normalized to the cut-off density n_{co} for $f = 72.8\,\mathrm{GHz}$. The black line indicates the nominal corrugated cut-off layer for this frequency. The fluctuation amplitude is $\sim 4\%$. The result of the full wave calculation for the upper DR antenna ($\theta_{tilt} = -18°$) is shown in Fig. 6c. The spectrum of the simulated density fluctuations (Fig. 6d) has a distinct peak at $k_\perp \sim 7\,\mathrm{cm}^{-1}$, which corresponds to $k_\perp \rho_s \sim 0.7$. This is close to the design value obtained from the Bragg condition for this frequency, $k_\perp^d = 9\,\mathrm{cm}^{-1}$. The simulation of the dynamic response of the reflected microwave signal is currently ongoing.

References

[1] Proll J, Trapped particle instabilities in quasi-aerodynamics stellarators, PhD thesis, EMAU Greifswald (2013).

[2] Marushchenko NB, Turkin Y, Maassberg H, Comp. Phys. Comm. **185**, 165 (2014).

[3] Hirsch M *et al.*, Nucl. Fusion **46** S853 (2006).

[4] Krämer-Flecken A, Soldatov S, Vowinkel B et al., Rev. Sci. Instrum. **81**, 113502 (2010).

[5] Rohmann P. et al. IEEE Int. Symposium on Phased Array Systems & Technology, 559 (2013).

[6] Lechte C, IEEE Trans. Plasma Sci., **37**, 1099 (2009).

[7] P. Xanthopoulos, H. Mynick, P. Helander, Y. Turkin *et al.*, Phys. Rev. Lett. **113**, 155001 (2014).